CF_3 Substitution of [Cu(P^P)(bpy)][PF_6] complexes: Effects on Photophysical Properties and Light-emitting Electrochemical Cell Performance

Sarah Keller,[a] Fabian Brunner,[a] José M. Junquera-Hernández,[b] Antonio Pertegás,[b] Maria-Grazia La-Placa,[b] Alessandro Prescimone,[a] Edwin C. Constable,[a] Henk J. Bolink,[b] Enrique Ortí*[b] and Catherine E. Housecroft*[a]

Abstract: We report [Cu(P^P)(N^N)][PF_6] complexes with P^P = bis(2-(diphenylphosphino)phenyl)ether (POP) or 4,5-bis(diphenylphosphino)-9,9-dimethylxanthene (xantphos), N^N = CF_3-substituted 2,2'-bipyridines (6,6'-$(CF_3)_2$bpy, 6-CF_3bpy, 5,5'-$(CF_3)_2$bpy, 4,4'-$(CF_3)_2$bpy, 6,6'-Me_2-4,4'-$(CF_3)_2$bpy). We present the effects of CF_3 substitution on structures, and electrochemical and photophysical properties. The HOMO–LUMO gap is tuned by the N^N ligand; the largest redshift in the MLCT band is for [Cu(P^P)(5,5'-$(CF_3)_2$bpy)][PF_6]. In solution, the compounds are weak yellow to red emitters. The emission properties depend on the substitution pattern but this cannot be explained by simple electronic arguments. For powders, [Cu(xantphos)(4,4'-$(CF_3)_2$bpy)][PF_6] has the highest PLQY (50.3%) with an emission lifetime of 12 μs. Compared to 298 K solution behaviour, excited state lifetimes lengthen in frozen Me-THF (77 K) indicating thermally activated delayed fluorescence (TADF). TD-DFT calculations show that the energy gap between the lowest-energy singlet and triplet excited states (0.12–0.20 eV) permits TADF. LECs with [Cu(POP)(6-CF_3bpy)][PF_6], [Cu(xantphos)(6-CF_3bpy)][PF_6] or [Cu(xantphos)(6,6'-Me_2-4,4'-$(CF_3)_2$bpy)][PF_6] emit yellow electroluminescence. A LEC with [Cu(xantphos)(6,6'-Me_2-4,4'-$(CF_3)_2$bpy)][PF_6] had the fastest turn-on time (8 min); the LEC with the longest lifetime ($t_{1/2}$ = 31 h) contained [Cu(xantphos)(6-CF_3bpy)][PF_6]; these LECs reached maximum luminances of 131 and 109 cd m^{-2}.

Introduction

The development of solid-state lighting based on the widely distributed organic light-emitting diodes (OLEDs) has had a massive impact on technology, especially for screens and displays.[1,2,3] Light-emitting electrochemical cells (LECs) are less well established, but are emerging devices which, like OLEDs, are based on the principle of electroluminescence. Compared to OLEDs, LECs are simpler in setup, more straight-forward in their processing and therefore also cheaper in production.[4] Whereas polymer-based or purely organic emitting materials are known for both LECs and OLEDs, the employment of transition metal complexes has certain advantages. Depending on the combination of different ligands and their substitution with functional groups, the properties of these metal complexes can be tuned in terms of emission colour, quantum yield and excited state lifetime.[5,6] For example, for $[Ir(ppy)_2(bpy)]^+$ (Hppy = 2-phenylpyridine, bpy = 2,2'-bipyridine) type complexes, different emission colours, photoluminescence quantum yields (PLQY) and device performances have been obtained upon modification of the cyclometallating Hppy or the ancillary bpy ligands.[5,6] Whereas iridium-based emitters can be extremely efficient,[7,8,9] their replacement by copper-based compounds has the advantage of higher abundance and therefore lower marked price of copper compared to iridium, which also translates to the costs of the devices.[10] Furthermore, many copper complexes are proven to exhibit thermally activated delayed fluorescence (TADF), a mechanism which allows the thermal population of the energetically higher singlet excited state from the triplet excited state. As a consequence, emission processes from all excited states are possible and in theory allow for quantum yields up to 100% to be reached.[11,12,13,14]

We have previously shown for [Cu(P^P)(bpy)][PF_6] complexes (where P^P = bis(2-diphenylphosphinophenyl)ether (POP) or 4,5-bis(diphenylphosphino)-9,9-dimethylxanthene (xantphos)), that the PLQY of the complex and the efficiency and lifetime in LEC devices are increased upon addition of methyl or ethyl groups in one or both 6-positions of the bpy ligand.[15,16] Costa *et al.*[17] systematically studied the effect of electron donating and electron withdrawing substituents at the 4-positions of bpy in [Cu(P^P)(bpy)][PF_6] complexes. The more negative the σ-Hammett parameter σ_p, which describes the σ-donation ability of a given substituent, the more enhanced is the performance of the LEC employing the respective compound, within a given series of complexes. We have demonstrated that the incorporation of

[a] S. Keller, F. Brunner, Dr. A. Prescimone, Prof. Dr. E.C. Constable, Prof. Dr. C.E. Housecroft
Department of Chemistry
University of Basel
BPR 1096, Mattenstrasse 24a, Basel 4058, Switzerland
E-mail: catherine.housecroft@unibas.ch
[b] Dr. J.M. Junquera, Dr. A. Pertegás, M.-G. La-Placa, Dr. H.J. Bolink, Prof. Dr. E. Ortí
Instituto de Ciencia Molecular,
Universidad de Valencia,
ES-45980 Paterna, Valencia, Spain
e-mail: enrique.orti@uv.es

Supporting information for this article is given via a link at the end of the document.

remote fluoro groups in [Cu(POP)(N^N)][PF_6] and [Cu(xantphos)(N^N)][PF_6], where N^N = 4,4'-bis(4-fluorophenyl)-6,6'-dimethyl-2,2'-bipyridine, leads to an enhancement of solid state and solution photophysical properties and is also beneficial to LEC performance.[18] This finding prompted us to investigate the potential positive effects that the introduction of CF_3 substituents may also have. Substitution with one or more trifluoromethyl groups is a common motif in coordination chemistry, especially for *N,N'*-chelating ligands incorporating pyrrole, pyrazole, triazole and tetrazole rings, as discussed for pyridyl azolates by Y. Chi *et al.*[19] Modification with CF_3 groups is often employed in luminescent materials containing Cu(I), Ir(III) and Pt(II) to Ru(II) and Os(II) complexes. However, CF_3-modified 2,2'-bipyridines are rarely mentioned in the literature, and copper complexes coordinated by a CF_3-substituted bpy are even more scarce.[20] The molar volume of a CF_3 group is significantly larger than for a methyl group and the steric effect is often comparable to that of an isopropyl group.[21] Furthermore, the electronic properties of methyl and CF_3 differ in that the former acts as a weak σ-donor whereas the latter has electron-withdrawing properties and therefore a more positive σ-Hammett parameter σ_p than alkyl groups.

Our aim in the present investigation was to prepare a series of copper(I) complexes of the type [Cu(POP)(bpy)][PF_6] and [Cu(xantphos)(bpy)][PF_6] with bpy ligands that are substituted with CF_3 groups in the 4-, 5- or 6-positions. The chemical structure of the POP, xantphos and bpy ligands used is given in Scheme 1. The electrochemical and photophysical properties of the new complexes are compared with those employing unsubstituted bpy as model compounds and with the Cu(I) complexes with alkyl-substituted bpy ligands,[16] and are interpreted with the help of density functional calculations. Those complexes with more promising photophysical properties are tested in LEC devices.

with C_{2v} symmetry for the complex cations containing symmetrically substituted bpy ligands.[16] The base peaks in the electrospray mass spectra match the respective [Cu(P^P)(N^N)]$^+$ cations, with isotope patterns agreeing with the calculated ones. Elemental analysis was performed to confirm the purity of the bulk compounds.

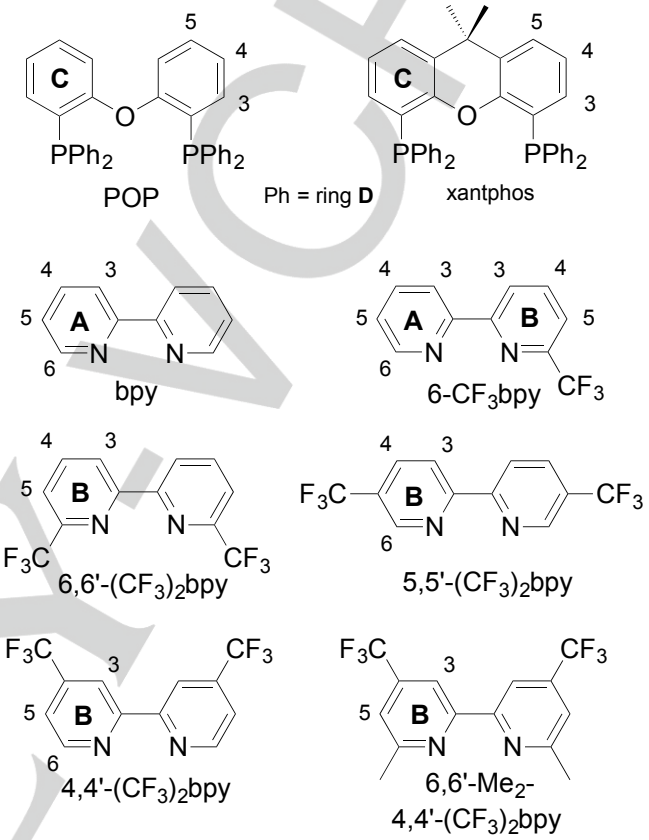

Scheme 1. Structures of ligands with ring and atom labels for NMR spectroscopic assignments.

Results and Discussion

Synthesis, stability and characterization of [Cu(P^P)(N^N)][PF_6] complexes

The [Cu(P^P)(N^N)][PF_6] complexes with P^P = POP and xantphos and N^N = bpy, 6-CF_3bpy, 5,5'-$(CF_3)_2$bpy and 4,4'-$(CF_3)_2$bpy, as well as the [Cu(xantphos)(6-Mebpy)][PF_6], [Cu(xantphos)(6,6'-Me_2bpy)][PF_6] and [Cu(xantphos)(6,6'-Me_2-4,4'-$(CF_3)_2$bpy)][PF_6] complexes (see Scheme 1 for ligands), were synthesized following the standard procedures[15,16,22] and were isolated as bright yellow to orange solids with yields of 52 to 96%. The formation of heteroleptic [Cu(P^P)(bpy)][PF_6] complexes was confirmed by one- and two-dimensional NMR spectroscopic techniques (^{1}H, ^{31}P, ^{19}F, ^{13}C, COSY, NOESY, HMQC, HMBC), which allowed for the unambiguous assignment of all signals. On the NMR spectroscopic timescale, the spectra of the compounds dissolved in acetone-d_6 are in accordance

Because of the constraints of the xanthene unit, the xantphos ligand is less sterically demanding than POP. As a consequence, the addition of the POP to [$Cu(MeCN)_4$]$^+$ leads to [Cu(POP)(MeCN)]$^+$ or [Cu(POP-*P,P'*)(POP-κ^1*P*)]$^+$. On the other hand, xantphos reacts with [$Cu(MeCN)_4$]$^+$ to give [Cu(xantphos-κ^2*P*)$_2$]$^+$.[23] This difference in behaviour leads to varying approaches to the preparation of [Cu(POP)(N^N)][PF_6] and [Cu(xantphos)(N^N][PF_6]. Whereas for complexes with POP, the bpy ligand was added after an initial reaction of POP and [$Cu(MeCN)_4$][PF_6] in CH_2Cl_2 (sequential addition),[15,16] for complexes with xantphos, a mixture of both the bisphosphane and the N^N ligand was added to the solution of [$Cu(MeCN)_4$][PF_6] to avoid formation of [$Cu(xantphos)_2$]$^+$ and facilitate the formation of heteroleptic [Cu(xantphos)(bpy)]$^+$.[16]

Substitution at the 6,6'-positions of the bpy ligand has a significant effect on both the photophysics and the stability of the [Cu(P^P)(bpy)]$^+$ complexes. Substituents in 6,6'-positions shield the copper(I) centre from solvent attack and

therefore reduce quenching by avoiding the so-called "solvent-related excited-state relaxations".[12,26] In general, large sterically demanding ligands in copper(I) complexes prevent a geometrical rearrangement of the tetrahedral cation towards more flattened structures upon excitation and thus help elongating excited state lifetimes. This structural effect was studied in detail for $[Cu(phen)_2]^+$ complexes.[24,25,26] However, if the substituents in the 6,6'-positions are too large or electronically repulsive, the exclusive formation of heteroleptic $[Cu(P\text{^}P)(N\text{^}N)]^+$ is not achievable and, instead, mixtures of homoleptic $[Cu(N\text{^}N)_2]^+$ and $[Cu(xantphos)_2]^+$ are obtained. This phenomenon has also been observed for complexes with phenanthrolines of different steric demand in the 2,9-positions together with a series of P^P chelating ligands.[27] Interestingly, substituents in the 4,4'-positions of the bpy ligand also appear to have an influence on the ligand redistribution (Scheme 2). For 6,6'-Me_2bpy, with 1.0 equivalents of xantphos and 1.2 equivalents of POP, respectively, an exclusive formation of the heteroleptic $[Cu(P\text{^}P)(bpy)]^+$ complexes was achieved (removal of excess P^P chelating ligand by subsequent layer crystallization (CH_2Cl_2/Et_2O).[16] In the case of 6,6'-Me_2-4,4'-$(CF_3)_2$bpy pure heteroleptic [Cu(xantphos)(6,6'-Me_2-4,4'-$(CF_3)_2$bpy)][PF_6] was obtained with 1.2 equivalents of xantphos (and following recrystallization to remove excess xantphos). However, the analogous reaction with POP leads to a mixture of free 6,6'-Me_2-4,4'-$(CF_3)_2$bpy and $[Cu(POP)_2][PF_6]$ with heteroleptic [Cu(POP)(6,6'-Me_2-4,4'-$(CF_3)_2$bpy)][PF_6], which we were not able to isolate without the side products and was therefore not characterized further (see Figure S1–S3 for NMR spectra).

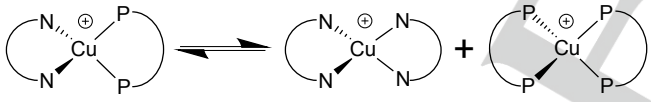

Scheme 2. Ligand redistribution results in an equilibrium between heteroleptic and homoleptic cations.

The sensitivity of the ligand redistribution equilibrium (Scheme 2) towards substituents in the 6,6'-positions of the bpy ligand was again corroborated by the unsuccessful attempts to isolate $[Cu(P\text{^}P)(6,6'\text{-}(CF_3)_2bpy)][PF_6]$ complexes. NMR spectra of the crude product of the reaction of $[Cu(MeCN)_4][PF_6]$ with POP (1.0 as well as 1.1 equivalents) in CH_2Cl_2 and subsequent addition of 6,6'-$(CF_3)_2$bpy identify the material as a mixture of $[Cu(POP)_2][PF_6]$, $[Cu(POP)(MeCN)_2][PF_6]$ and $[Cu(6,6'\text{-}(CF_3)_2bpy)_2][PF_6]$.[28] In the mass spectrum, the base peak at *m/z* 601.2 was assigned to $[Cu(POP)]^+$, and no peak envelope arising from $[Cu(POP)(6,6'\text{-}(CF_3)_2bpy)]^+$ was detected.

The attempted synthesis of [Cu(xantphos)(6,6'-$(CF_3)_2$bpy)][PF_6] from $[Cu(MeCN)_4][PF_6]$, 6,6'-$(CF_3)_2$bpy and xantphos (1.0 as well as 1.2 equivalents) in CH_2Cl_2 yielded a pale orange solid upon solvent removal. NMR spectroscopic data for the crude product showed a mixture of $[Cu(xantphos)(MeCN)_2]^+$ and $[Cu(6,6'\text{-}(CF_3)_2bpy)_2][PF_6]$.[28] In the electrospray mass spectrum, peak envelopes at *m/z* 641.3 and 1219.7 were assigned to $[Cu(xantphos)]^+$ and $[Cu(xantphos)_2]^+$, but no ion attributed to $[Cu(xantphos)(6,6'\text{-}(CF_3)_2bpy)]^+$ was observed. Layer recrystallization (CH_2Cl_2/Et_2O) of the crude material led to a mixture of colourless (dominant) and orange crystals, which could be manually separated. While the orange crystals were identified as homoleptic $[Cu(6,6'\text{-}(CF_3)_2bpy)_2][PF_6]$,[28] analysis of the colourless crystals showed the formation of a one-dimensional coordination polymer [{Cu(xantphos)(μ-PO_2F_2)}$_n$], with the copper centres linked by μ-PO_2F_2 units which stem from partial hydrolysis of the $[PF_6]^-$ anion.[29]

Closer inspection of the spatial properties of the CF_3 group helps us to understand why the formation of the heteroleptic $[Cu(P\text{^}P)(6,6'\text{-}(CF_3)_2bpy)][PF_6]$ complexes was not successful. Whereas the calculated van der Waals radius for a methyl group lies between 1.715 and 2.230 Å, the reported values for a CF_3 group are between 2.107 and 2.743 Å.[30] Although the van der Waals radius is a reasonable parameter to compare, it is only an intrinsic property. In order to determine the steric effect, which is an extrinsic phenomenon, coulombic interactions between all the atoms or groups involved in the interaction have to be taken into consideration. A number of different approaches to analyse the steric effect of typical substituents show that a CF_3 group is comparable with an isopropyl group.[21,31] Considering that two ethyl groups in the 6,6'-positions at the bpy are already too sterically demanding to allow the exclusive formation of heteroleptic $[Cu(P\text{^}P)(6,6'\text{-}Et_2bpy)]^+$ cations, the steric requirements of two CF_3 groups are way beyond what these type of heteroleptic $[Cu(P\text{^}P)(bpy)][PF_6]$ complexes can offer.

In the case of unsubstituted bipyridine, $[Cu(POP)(bpy)][PF_6]$ was previously synthesized and characterized.[Error! Bookmark not defined.] In contrast, $[Cu(xantphos)(bpy)]^+$ has only been reported as the $[BF_4]^-$ salt.[22] We decided that $[Cu(POP)(bpy)][PF_6]$ and $[Cu(xantphos)(bpy)][PF_6]$ would serve well as reference complexes to compare the effects of attaching CF_3 and methyl groups in different positions in the bpy ligand. $[Cu(xantphos)(6,6'\text{-}Me_2bpy)][PF_6]$ and [Cu(xantphos)(6-Mebpy)][PF_6] were investigated in an earlier study[16] and are included here for comparative purposes.

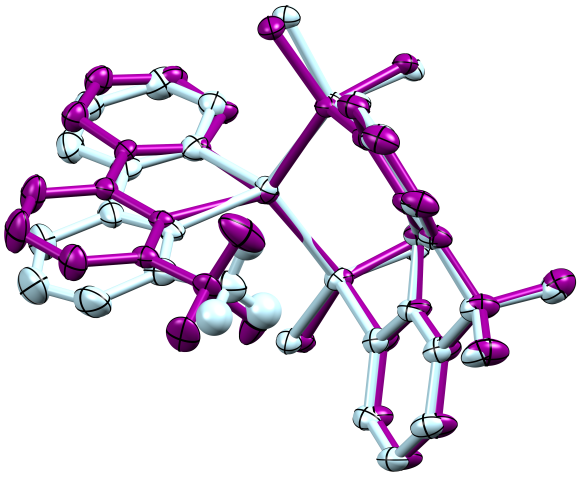

Figure 1. Overlay of the molecular structures of $[Cu(xantphos)(6\text{-}Mebpy)]^+$ (light blue) and the major conformation of $[Cu(xantphos)(6\text{-}CF_3bpy)]^+$ (purple) with ellipsoids plotted at 50% probability level. Only the ipso-C atoms of the PPh_2 phenyl rings are shown and H atoms are omitted, with exception of the methyl group at the bipyridine to allow for a better comparison with the CF_3 group. The Cu atoms, pairs of corresponding N atoms and corresponding P atoms were overlaid.

Structural characterization

X-ray quality crystals of $[Cu(xantphos)(bpy)][PF_6]$, $[Cu(POP)(6\text{-}CF_3bpy)][PF_6]\cdot 1.3Et_2O\cdot 0.35H_2O$, $[Cu(xantphos)(6\text{-}CF_3bpy)][PF_6]\cdot 2Et_2O\cdot 1.5CH_2Cl_2$, $[Cu(POP)(4,4'\text{-}(CF_3)_2bpy)][PF_6]\cdot 0.5CH_2Cl_2$, $[Cu(xantphos)(4,4'\text{-}(CF_3)_2bpy)][PF_6]$ and $[Cu(POP)(5,5'\text{-}(CF_3)_2bpy)][PF_6]\cdot 0.5Et_2O$ were grown by layering Et_2O over CH_2Cl_2 solutions of the compounds. ORTEP-style diagrams of the cations in the complexes are illustrated in Figure S4-S9 in the Supporting Information. We compare these structures to those published for $[Cu(POP)(bpy)][PF_6]\cdot CHCl_3$,[Error! Bookmark not defined.] $[Cu(xantphos)(6\text{-}Mebpy)][PF_6]\cdot CH_2Cl_2\cdot 0.4Et_2O$ and $[Cu(xantphos)(6,6'\text{-}Me_2bpy)][PF_6]$.[16] Most of the complexes crystallize in the triclinic space group *P*−1, with the exception of $[Cu(xantphos)(bpy)][PF_6]$ and $[Cu(POP)(bpy)][PF_6]\cdot CHCl_3$ (both monoclinic $P2_1/n$) and $[Cu(POP)(5,5'\text{-}(CF_3)_2bpy)][PF_6]\cdot 0.5Et_2O$ (monoclinic $P2_1/c$). The Cu–P and Cu–N bond distances show little variation and are found to be within 2.2159(11) and 2.2841(10) Å, and between 2.014(2) and 2.1523(19) Å, respectively. Whereas the N–Cu–N angles in all of the complexes stay very close to 80° (79.25(9) – 80.97(12)°), the P–Cu–P chelating angles range from 111.87(3) to 119.47(3)° for the complexes with POP and from 113.38(3) to 122.58(4)° for those with xantphos. In the case of the unsymmetrical $[Cu(xantphos)(6\text{-}CF_3bpy)]^+$ cation, the 6-CF_3bipy ligand is disordered over two orientations with occupancies of 0.75 (CF_3 group facing towards the xanthene "bowl") and 0.25 (CF_3 away from the xanthene "bowl"), respectively. The major conformation is identical to the one reported for the $[Cu(xantphos)(6\text{-}Mebpy)]^+$ cation.[16] In Table 1, the dihedral angle between the planes through N–Cu–N and P–Cu–P illustrates the distortion from the orthogonal coordination of the two ligands. Whereas $[Cu(xantphos)(bpy)]^+$ and $[Cu(POP)(6\text{-}CF_3bpy)]^+$ show the largest distortion (79.63 and 79.03°, respectively), the cations where the angle comes closest to 90° are $[Cu(POP)(bpy)]^+$ (88.52°) and $[Cu(xantphos)(6\text{-}Mebpy)]^+$ (87.92°). It appears that the dihedral angle is predominantly influenced by packing effects since no clear trend within the series of bpy ligands or upon exchange of POP and xantphos could be identified. The dihedral N–C–C–N angle defining the interring rotation of the bpy ligands varies from no torsion at all (0(1)°) for $[Cu(POP)(4,4'\text{-}(CF_3)_2bpy)]^+$ to a significant torsion of 20.5(2)° for $[Cu(xantphos)(bpy)]^+$. It is worth pointing out that the parameters for $[Cu(xantphos)(6\text{-}CF_3bpy)]^+$ are very close to those of $[Cu(xantphos)(6\text{-}Mebpy)]^+$, which is also illustrated in the structure overlay of the two cations in Figure 1.

Table 1. Comparison of structural parameters of the $[Cu(P\text{^}P)(N\text{^}N)]^+$ cations

Complex cation	P–Cu–P chelating angle / deg	N–Cu–N chelating angle / deg	Angle between P–Cu–P and N–Cu–N planes / deg	N–C–C–N torsion angle /deg
$[Cu(POP)(bpy)]^+$ [a]	119.47(3)	79.66(7)	88.52	–2.8(3)
$[Cu(xantphos)(bpy)]^+$	113.816(14)	79.32(5)	79.63	20.5(2)
$[Cu(POP)(6\text{-}CF_3bpy)]^+$	115.68(3)	80.35(10)	79.03	–18.3(4)
$[Cu(xantphos)(6\text{-}CF_3bpy)]^+$	113.55(3)	79.93(9)	86.61	0.6(4)
$[Cu(POP)(5,5'\text{-}(CF_3)_2bpy)]^+$	111.87(3)	79.25(9)	83.54	6.2(3)
$[Cu(POP)(4,4'\text{-}(CF_3)_2bpy)]^+$	113.02(5)	79.7(2)	85.83	0(1)
$[Cu(xantphos)(4,4'\text{-}(CF_3)_2bpy)]^+$	122.58(4)	79.63(13)	84.63	–17.2(5)
$[Cu(xantphos)(6\text{-}Mebpy)]^+$ [a]	113.38(3)	80.97(12)	87.92	1.7(5)
$[Cu(xantphos)(6,6'\text{-}Me_2bpy)]^+$ [a]	119.47(3)	79.66(9)	85.48	6.7(3)

[a] Published data for $[Cu(POP)(bpy)][PF_6]\cdot CHCl_3$,[Error! Bookmark not defined.] $[Cu(xantphos)(6\text{-}Mebpy)][PF_6]\cdot CH_2Cl_2\cdot 0.4Et_2O$ and $[Cu(xantphos)(6,6'\text{-}Me_2bpy)][PF_6]$.[16]

Electrochemistry

Cyclic voltammetry was used to characterize the redox properties of the copper(I) cations (Table 2), and a representative cyclic voltammogram of $[Cu(POP)(4,4'\text{-}(CF_3)_2bpy)][PF_6]$ is illustrated in Figure S10 in the Supporting Information. The lowest oxidation potential $E_{1/2}^{ox}$ (vs. Fc^+/Fc), which corresponds to a Cu^+/Cu^{2+} process, was observed at +0.72 and +0.76 V for the reference complexes $[Cu(POP)(bpy)][PF_6]$ and $[Cu(xantphos)(bpy)][PF_6]$, respectively. The substituted complexes present $E_{1/2}^{ox}$ values between +0.85 and +0.96 V, the highest value corresponding to

[Cu(xantphos)(6,6'-Me_2-4,4'-$(CF_3)_2$bpy)][PF_6]. In comparison to the other complexes, which have potential separations (E_{pc} – E_{pa}) between 100 and 180 mV, a significantly larger separation of 280 mV was recorded for [Cu(xantphos)(6,6'-Me_2-4,4'-$(CF_3)_2$bpy)][PF_6]. All complexes show a second oxidation peak at around +1.2 V which corresponds to an oxidation of the phosphane ligand (Figure S10). The second reduction peak at around +0.1 V is connected to this overoxidation; it is not visible when the scan is recorded only up to +1.0 V and only the first oxidation is accessed. The complexes with CF_3-modified bpy ligands show reduction processes in addition to the typical oxidation process, which is in contrast to similar complexes with unsubstituted or alkyl-substituted bpy ligands. For the complexes with two CF_3 groups at the bipyridine, this reduction is located around –1.6 V, whereas for the complexes with mono-substituted 6-CF_3bpy this value is cathodically shifted being around –1.9 V.

Table 2. Cyclic voltammetric data for [Cu(N^N)(P^P)][PF_6] complexes referenced to internal Fc/Fc^+ = 0.V; CH_2Cl_2 (freshly distilled) solutions with [$^nBu_4N$][PF_6] as supporting electrolyte and scan rate of 0.1 V s^{-1}. Processes are quasi-reversible.

Complex cation	$E_{1/2}^{ox}$ / V (E_{pc} – E_{pa} / mV)	$E_{1/2}^{red}$ / V	ΔE /V
[Cu(POP)(bpy)]$^+$	+0.72 (110)	–	–
[Cu(xantphos)(bpy)]$^+$	+0.76 (110)	–	–
[Cu(POP)(6-CF_3bpy)]$^+$	+0.90 (170)	–1.94	2.84
[Cu(xantphos)(6-CF_3bpy)]$^+$	+0.92 (100)	–1.89	2.81
[Cu(POP)(5,5'-$(CF_3)_2$bpy)]$^+$	+0.89 (150)	–1.59	2.48
[Cu(xantphos)(5,5'-$(CF_3)_2$bpy)]$^+$	+0.94 (180)	–1.55	2.49
[Cu(POP)(4,4'-$(CF_3)_2$bpy)]$^+$	+0.88 (110)	–1.66	2.54
[Cu(xantphos)(4,4'-$(CF_3)_2$bpy)]$^+$	+0.92 (140)	–1.62	2.54
[Cu(xantphos)(6,6'-Me_2-4,4'-$(CF_3)_2$bpy)]$^+$	+0.96 (280)	–1.67	2.63
[Cu(xantphos)(6-Mebpy)]$^+$	+0.85 (100)	–	–
[Cu(xantphos)(6,6'Me_2bpy)]$^+$	+0.90 (150)	–	–

Ground state theoretical calculations

The geometry of all the [Cu(N^N)(P^P)]$^+$ cations in their ground electronic state S_0 was optimized at the DFT B3LYP/(6-31**G+LANL2DZ) level without imposing any symmetry restriction. Table S1 in the Supporting Information summarizes the values calculated for selected structural parameters. Calculations satisfactorily reproduce the distorted-tetrahedral configuration defined by the P^P and N^N ligands around the metal centre. The Cu−P bond lengths range from 2.368 to 2.433 Å, and the Cu−N bond lengths are between 2.152 and 2.276 Å, slightly overestimating (~0.1 Å) the reported X-ray values (Table 1). The N−Cu−N and P−Cu−P chelating angles present values between 75.38 and 77.26º and between 113.71 and 116.89º, respectively, and slightly underestimate the X-ray values. The angle between the planes through N–Cu–N and P–Cu–P illustrating the distortion from the orthogonal coordination of the two ligands is in a range between 85 and 90º, which is slightly narrower than that observed experimentally. It should be stressed that the theoretical geometries correspond to minimum-energy structures optimized in solution and do not take into account the packing forces acting in the solid state. These forces tend to reduce the coordination distances and to increase the chelating angles.

Figure 2 sketches the evolution of the energy calculated for the highest-occupied (HOMO) and lowest-unoccupied molecular orbital (LUMO) along the series of complexes studied. The topology of the molecular orbitals does not vary significantly along the series, so only the contour plots for the reference complexes [Cu(xantphos)(bpy)]$^+$ and [Cu(POP)(bpy)]$^+$ are shown in Figure 2. As previously found for this type of complexes,[16,Error! Bookmark not defined.] the HOMO appears mainly centred on the metal with a small contribution from the phosphorus atoms, whereas the LUMO spreads over the bpy ligand. The energy of the HOMO slightly changes along both series being between –6.03 and –6.19 eV. This small change is an expected result, because the HOMO is centred on a region of the complex that remains structurally unchanged along the series, and is consistent with the small variation observed in the oxidation potentials of the substituted complexes (0.85–0.96 V). The attachment of CF_3 groups in 4,4'- and 5,5'-positions of the bpy causes a small stabilization of the HOMO (~0.1 eV) in good agreement with the higher oxidation potentials measured experimentally for these complexes (Table 2). Substitution of POP by xantphos also leads to a small stabilization of the HOMO (~0.05 eV) in accord with the slightly more positive oxidation potentials recorded for the xantphos derivatives.

As shown in Figure 2, the energy of the LUMO features larger changes because the attachment of electron-withdrawing CF_3 groups to the bpy ligand, where the LUMO is located, provokes the stabilization of this orbital. The addition of a single CF_3 group stabilizes the LUMO by around 0.2 eV, whereas the introduction of a second group causes an additional stabilization of 0.3 eV. The effect is slightly larger (0.07eV) when substitution is made in 5,5'-positions compared with 4,4'-positions. The introduction of electron-donor methyl groups in [Cu(xantphos)(N^N)]$^+$ is the contrary, inducing a small destabilization of the LUMO of 0.04 eV upon introduction of the first Me in passing from [Cu(xantphos)(bpy)]$^+$ to [Cu(xantphos)(6-Mebpy)]$^+$, and of 0.12 eV after introducing the second group in [Cu(xantphos)(6,6'-Me_2bpy)]$^+$. In the complex cation [Cu(xantphos)(6,6'-Me_2-4,4'-$(CF_3)_2$bpy)]$^+$, where both CF_3 and Me groups are added, the effects sum up and the LUMO appears 0.12 eV higher in energy than that of

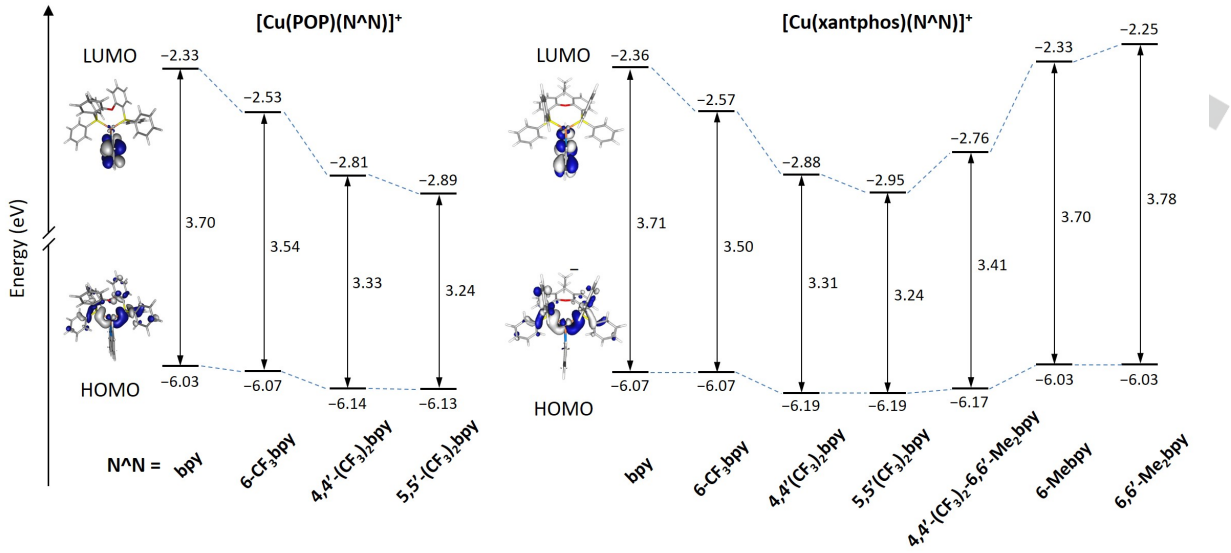

Figure 2. Energy diagram showing the energies calculated for the HOMO and LUMO of $[Cu(POP)(N^N)]^+$ and $[Cu(xantphos)(N^N)]^+$ complexes. The HOMO−LUMO energy gap is also quoted. Isovalue contour plots (±0.03 a.u.) are shown for the HOMO and LUMO of the reference complexes (N^N = bpy)

$[Cu(xantphos)(4,4'\text{-}(CF_3)_2bpy)]^+$. The trends predicted for the energy of the LUMO perfectly explain the reduction potentials discussed above for complexes including CF_3 groups (Table 2). In summary, complexes incorporating the 6-CF_3bpy ligand present a more negative potential than complexes bearing two CF_3 groups, and, within the latter, complexes substituted in 4,4'-positions show less negative potentials (by 0.07 V) than complexes substituted in 5,5'-positions due to the LUMO stabilization (0.07 eV) in passing from 4,4'- to 5,5'-substituted derivatives.

The smallest HOMO−LUMO energy gap (3.24 eV) is obtained for $[Cu(POP)(5,5'\text{-}(CF_3)_2bpy)]^+$ and $[Cu(xantphos)(5,5'\text{-}(CF_3)_2bpy)]^+$, followed by those calculated for $[Cu(xantphos)(4,4'\text{-}(CF_3)_2bpy)]^+$ (3.31 eV), $[Cu(POP)(4,4'\text{-}(CF_3)_2bpy)]^+$ (3.33 eV) and $[Cu(xantphos)(6,6'\text{-}Me_2\text{-}4,4'\text{-}(CF_3)_2bpy)]^+$ (3.41 eV). Complexes $[Cu(xantphos)(6\text{-}CF_3bpy)]^+$ and $[Cu(POP)(6\text{-}CF_3bpy)]^+$ with a single CF_3 group feature intermediate gap values of 3.50 and 3.54 eV, respectively, and the widest gaps correspond to unsubstituted or Me-substituted complexes with values in the 3.70–3.78 eV range (Figure 2). These trends correctly reproduce the relative order of the electrochemical gaps inferred from redox potentials (Table 1).

The HOMO−LUMO gap can be used, in a first approach, to predict the relative energy of the lowest-energy singlet (S_1) and triplet (T_1) electronic excited states, usually described by the HOMO→LUMO excitation in this type of complexes. On this basis, unsubstituted and Me-substituted complexes will be the ones featuring S_1 and T_1 at higher energies and bluer absorption/emission wavelengths. These wavelengths will shift to the red as CF_3 groups are added, the maximum shift being expected for complexes bearing the 5,5'-$(CF_3)_2$bpy ligand which show the lowest HOMO−LUMO gap. However, it has to be considered that, although this energy ordering may be correct at the ground state optimum geometries (Franck-Condon region), geometry relaxation of the excited state cannot be ignored when dealing with emission processes as discussed below.

Photophysical properties and excited states

The UV-Vis absorption spectra of CH_2Cl_2 solutions of the $[Cu(P^P)(bpy)][PF_6]$ complexes show, in addition to ligand-centred bands around 280 nm, very broad bands in the region between 350 and 480 nm, that are assigned to MLCT transitions (Figure 3, Table 3 and Figure S11). For a given bpy, the MLCT absorption bands of the respective complexes with POP and xantphos are very similar in both the value of λ_{max} and the shape of the band. This suggests that the energy difference between the HOMO and the LUMO is mainly determined by the *N,N'*-chelating ligand in accord with the DFT results discussed above. Since the HOMO is fully located on the {Cu(P^P)} domain and is similar for all the complexes, we can directly observe the effect of the substitution pattern in the bpy ligand on the

HOMO−LUMO gap from the MLCT maxima. Because of the similarity of the absorption spectra between the respective pairs of POP and xantphos complexes, we focus only on the series of xantphos complexes and compare this group to [Cu(xantphos)(bpy)][PF_6] with unsubstituted bpy as the model compound. All of the complexes with one or more CF_3 groups at the bpy show a redshift with respect to [Cu(xantphos)(bpy)][PF_6], corroborating the energy lowering of the LUMO and the smaller HOMO–LUMO gap predicted theoretically. The largest redshift of 400 meV (54 nm) is observed for [Cu(xantphos)(5,5'-$(CF_3)_2$bpy)][PF_6] and the smallest comes to 153 meV (19 nm) for [Cu(xantphos)(6-CF_3bpy)][PF_6] (see also Table S2), in perfect agreement with the HOMO−LUMO gaps calculated for these complexes. Substitution of the bpy ligand with one or two methyl groups in the 6-positions results in a blueshift of 17 and 69 meV (2 and 8 nm) for the respective complex, in accord with the destabilization of the LUMO and the increase of the HOMO–LUMO distance.

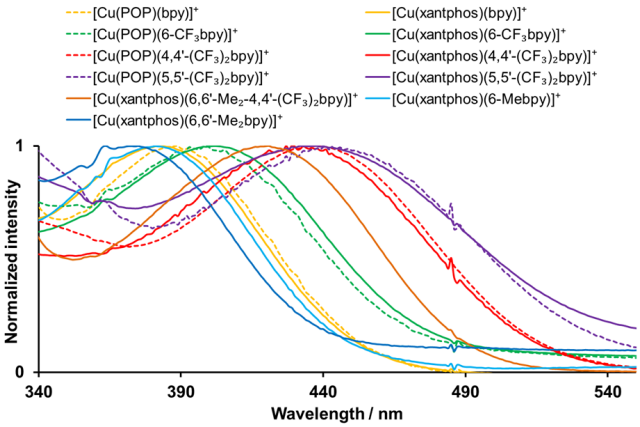

Figure 3. Expansion of the lowest-energy MLCT region of the normalized solution absorption spectra of the [Cu(P^P)(N^N)][PF_6] complexes (CH_2Cl_2, 2.5 × 10^{-5} mol dm^{-3}). For the full spectrum see Figure S10, and for a comparison of the maxima, see Table S2.

To gain a deeper insight into the nature of the electronic excited states giving rise to the absorption spectra, singlet (S_n) and triplet (T_n) excited states were calculated for all the complexes using the time dependent DFT (TD-DFT) approach. Table 4 summarizes the vertical excitation energies computed for the lowest-energy singlet (S_1) and triplet (T_1) states at the optimized geometry of S_0. For all the complexes, both S_1 and T_1 result from the HOMO→LUMO monoexcitation with a contribution always exceeding 90%. This supports the MLCT

Table 3. Absorption and emission maxima, photoluminescence quantum yields (PLQY) and lifetimes ($\tau_{1/2}$) for [Cu(P^P)(N^N)][PF_6] complexes.

Complex cation	CH_2Cl_2 solution[a]					Powder[b]			Me-THF at 77 K	
	UV-Vis MLCT λ^{max} / nm	λ_{exc} / nm	λ_{em}^{max} / nm	PLQY (non-deaerated / deaerated) / %	$\tau_{1/2}$ (non-deaerated / deaerated) / ns	λ_{em}^{max} / nm	PLQY / %	$\tau_{1/2}$ / µs	λ_{em}^{max} / nm	$\tau_{1/2}$ / µs
[Cu(POP)(bpy)]+ [e]	388	388	618, 649[a]	0.4/0.5	43/46	581[c]	3.0[c]	1.5[c]	610	16
[Cu(xantphos)(bpy)]+	383	390	620, 650[a]	0.5/0.5	75/104	587[c]	1.7[c]	1.3[c]	613	11
[Cu(POP)(6-CF_3bpy)]+	399	380	618, 646[a]	0.7/0.7	95/119	575[c]	6.2[c]	2.9[c]	610	45
[Cu(xantphos)(6-CF_3bpy)]+	402	380	622, 647[a]	0.6/0.6	84/99	581[c]	11.1[c]	2.9[c]	595	31
[Cu(POP)(5,5'-$(CF_3)_2$bpy)]+	441	-	-	-/-	-/-	648	0.5[d]	0.185[d]	656	––
[Cu(xantphos)(5,5'-$(CF_3)_2$bpy)]+	437	-	-	-/-	-/-	647	0.5[d]	0.251[d]	646	––
[Cu(POP)(4,4'-$(CF_3)_2$bpy)]+	436	430	667, 697[b] (very weak)	-/-	-/-	664[d]	0.5[d]	0.096[d]	650	3
[Cu(xantphos)(4,4'-$(CF_3)_2$bpy)]+	433	430	667, 705[b] (very weak)	-/-	-/-	632[d]	0.9[d]	0.579[d]	652	5
[Cu(xantphos)(6,6'-Me_2-4,4'-$(CF_3)_2$bpy)]+	421	400	612, 637[a]	0.5/0.5	39/39	517[c]	50.3[c]	12[c]	604	42
[Cu(xantphos)(6-Mebpy)]+	381	379	605, 635[a]	1.0/1.8	27/78	547[c]	33.8	9.6[c]	567	46
[Cu(xantphos)(6,6'-Me_2bpy)]+	375	379	606, 635[a]	1.6/10.0	451/3406	539[c]	37.3[c]	11.4[c]	551	88

[a]Solution concentration = 2.5 × 10^{-5} mol dm^{-3}. [b]Solution concentration = 5.0 × 10^{-5} mol dm^{-3}. [c]λ_{exc} = 365 nm. [d]λ_{xc} = 405 nm. Deaeration was by flow of argon. [e][Cu(POP)(bpy)][PF_6] was prepared according to the literature (ref. 43) but measurements were made for the present work.

character of the S_1 and T_1 states since the HOMO→LUMO excitation implies an electron transfer from the {Cu(P^P)} environment to the bpy ligand (see Figure 2). The oscillator strength (*f*) calculated for the electronic transition to the S_1 state lies between 0.06 and 0.13 (Table 4), the next singlet excited state with *f* values higher than 0.01 being around 0.9 eV above S_1. Excited states with high oscillator strengths (~0.40), centred on the ligands, are found around 285 nm (~4.35 eV) in good agreement with the intense bands observed in this region in the absorption spectrum. These results identify the S_1 state as responsible of the low-energy absorption band observed in the spectra in the 350–500 nm region (Figures 3 and S11). The vertical excitation energies calculated for S_1 (Table 4) are in good agreement with the absorption maxima correctly reproducing the experimental trends (Table 3). Complexes with Me substituents feature S_1 energies blue shifted with respect to the reference complexes, whereas S_1 states of complexes with one or two CF_3 groups appears gradually shifted to the red. The lowest excitation energy is predicted for [Cu(POP)(5,5'-$(CF_3)_2$bpy)]$^+$ (2.65 eV, 468 nm) and [Cu(xantphos)(5,5'-$(CF_3)_2$bpy)]$^+$ (2.66 eV, 467 nm) in very good agreement with experimental λ^{max} values (441 and 437 nm, respectively). The [Cu(xantphos)(6,6'-Me_2-4,4'-$(CF_3)_2$bpy)]$^+$ complex presents an excitation energy (2.80 eV, 442 nm) lower than the [Cu(xantphos)(4,4'-$(CF_3)_2$bpy)]$^+$ complex (2.71 eV, 457 nm) due to the presence of methyl groups. The energy ordering of the S_1 states also agrees with that expected from the MO analysis and the electrochemical gaps, and corroborates that light absorption, which takes place around the ground state optimal geometry, can be explained based on electronic factors without considering the flattening effects that the HOMO→LUMO excitation has on the molecular geometry of the excited states as explained below. The T_1 states are computed 0.16–0.20 eV below S_1 (Table 4) and the vertical excitation energies to T_1 follow the same trends discussed above for S_1.

Table 4. Vertical excitation energies (*E*) calculated at the TD-DFT B3LYP/(6-31G**+LANL2DZ) level for the lowest singlet (S_1) and triplet (T_1) excited states of complexes [Cu(N^N)(P^P)]$^+$ in CH_2Cl_2 solution. S_0→S_1 oscillator strengths (*f*) are given within parentheses.

Complex cation	S_1	T_1
	E (eV/nm) (*f*)	*E* (eV)
[Cu(POP)(bpy)]$^+$	3.089 / 401 (0.08)	2.906
[Cu(xantphos)(bpy)]$^+$	3.085 / 402 (0.09)	2.893
[Cu(POP)(6-CF_3bpy)]$^+$	2.930 / 423 (0.06)	2.772
[Cu(xantphos)(6-CF_3bpy)]$^+$	2.874 / 431 (0.07)	2.704
[Cu(POP)(5,5'-$(CF_3)_2$bpy)]$^+$	2.647 / 468 (0.06)	2.484
[Cu(xantphos)(5,5'-$(CF_3)_2$bpy)]$^+$	2.655 / 467 (0.07)	2.483
[Cu(POP)(4,4'-$(CF_3)_2$bpy)]$^+$	2.739 / 453 (0.09)	2.531
[Cu(xantphos)(4,4'-$(CF_3)_2$bpy)]$^+$	2.713 / 457 (0.13)	2.512
[Cu(xantphos)(6,6'-$Me_2$4,4'-$(CF_3)_2$-bpy)]$^+$	2.802 / 442 (0.11)	2.639
[Cu(xantphos)(6-Mebpy)]$^+$	3.088 / 402 (0.09)	2.896
[Cu(xantphos)(6,6'-Me_2bpy)]$^+$	3.145 / 394 (0.06)	2.985

Figure 4 illustrates the normalized solution emission spectra of the [Cu(P^P)(bpy)][PF_6] complexes in CH_2Cl_2 upon excitation in the region of their respective MLCT band; values of λ_{em}^{max} are presented in Table 3. Due to their poor emissive behaviour, the spectra of the complexes with 4,4'-$(CF_3)_2$bpy are not included in Figure 3. The complexes with 5,5'-$(CF_3)_2$bpy were non-emissive in solution. With emission maxima between 605 and 705 nm, the complexes are yellow to red emitters in solution. The bands are structured with two maxima, and as in the absorption spectra, the emission bands are only slightly affected by a change from POP to xantphos for a given N^N ligand. In contrast to the absorption spectra where a redshift was observed, the emission of complexes with 6-CF_3bpy remains almost unchanged with respect to the unsubstituted complexes and that of complex with 6,6'-Me_2-4,4'-$(CF_3)_2$bpy is slightly blueshifted. The largest blueshift is recorded for the complexes with 6-Mebpy and 6,6'-Me_2bpy.

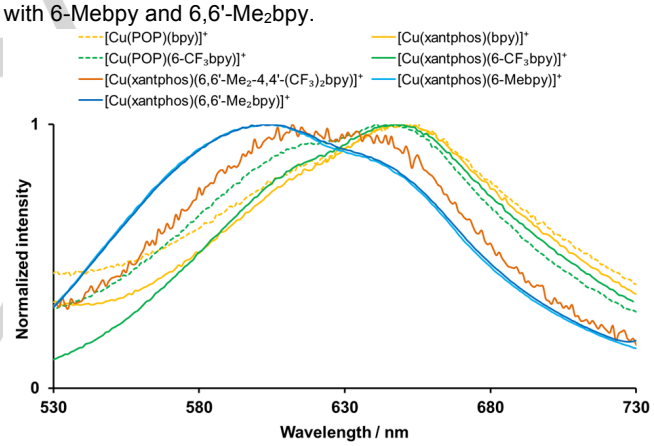

Figure 4. Solution emission spectra of [Cu(P^P)(N^N)][PF_6] complexes (CH_2Cl_2, 2.5 × 10^{-5} mol dm^{-3}). For λ_{exc} see Table 3.

The solid-state (powder) emission spectra for all complexes are shown in Figure 5. The only complexes where the emission is redshifted with respect to the spectra of the complexes with unsubstituted bpy are those with 5,5'-$(CF_3)_2$bpy and 4,4'-$(CF_3)_2$bpy. The redshift is more pronounced for the complexes with POP, being 83 nm for [Cu(POP)(4,4'-$(CF_3)_2$bpy)][PF_6] and 67 nm for [Cu(POP)(5,5'-$(CF_3)_2$bpy)][PF_6] (Table 3). The emission maxima of [Cu(POP)(6-CF_3bpy)][PF_6] and [Cu(xantphos)(6-CF_3bpy)][PF_6] both are shifted 6 nm to shorter wavelengths. In contrast to the solution emission spectra, where complexes with 6-Mebpy and 6,6'-Me_2bpy exhibit the largest shift to shorter wavelengths, the complex with the most blueshifted (70 nm) solid state emission is [Cu(xantphos)(6,6'-Me_2-4,4'-$(CF_3)_2$bpy)][PF_6].

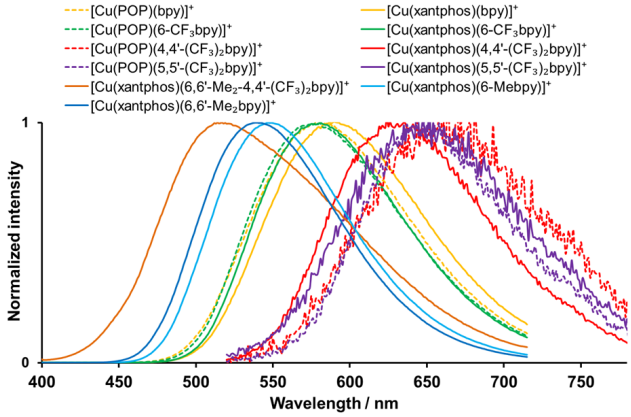

Figure 5. Normalized powder emission spectra of [Cu(P^P)(N^N)][PF_6] complexes. For λ_{exc} see Table 3.

In order to visualize the solid state emission, photographs of the powder samples of [Cu(xantphos)(N^N)][PF_6] under normal and under UV light (λ_{exc} = 365 nm) are shown in Figure 6. Solid [Cu(xantphos)(5,5'-$(CF_3)_2$bpy)][PF_6] appears nearly non-emissive, (consistent with the low solid-state PLQY, Table 3). Overall, the photophysical properties of both POP and xantphos complexes with 5,5'-$(CF_3)_2$bpy are impaired with respect to their respective reference complexes with naked bpy, and we have to conclude that a modification with CF_3 groups in this position is not beneficial for emissive applications. With PLQY = 0.9%, the weak red emission of solid [Cu(xantphos)(4,4'-$(CF_3)_2$bpy)][PF_6] is just visible by eye (Figure 6). However, even for a red emitter this value is too low to qualify this complex as luminophore, and as a result the 4,4'-substitution of the bpy ligand with CF_3 groups appears detrimental. In contrast, [Cu(POP)(6-CF_3bpy)][PF_6] and [Cu(xantphos)(6-CF_3bpy)][PF_6] have increased PLQY and lifetime values, both in solution and in powder, when compared to their respective reference complexes [Cu(POP)(bpy)][PF_6] and [Cu(xantphos)(bpy)][PF_6]. Whereas the powder PLQY is only doubled for [Cu(POP)(6-CF_3bpy)][PF_6] (6.2% in comparison to 3.0% for the model compound), the value is more than six times higher for [Cu(xantphos)(6-CF_3bpy)][PF_6] (11.1% versus 1.7%). Although the CF_3 group in the 6-position of the bpy appears to be beneficial for the photophysical properties, it is less efficient than a methyl group in this position (PLQY 9.5% for [Cu(POP)(6-Mebpy)][PF_6],[15] and 33.8% for [Cu(xantphos)(6-Mebpy)][PF_6]).[16]

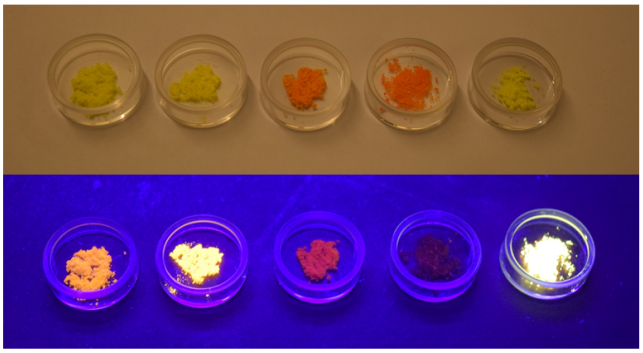

Figure 6. Powder samples of [Cu(xantphos)(N^N)][PF_6] complexes under normal light (top) and under UV light (λ_{exc} = 365 nm, bottom). From left to right: [Cu(xantphos)(bpy)][PF_6], [Cu(xantphos)(6-CF_3bpy)][PF_6], [Cu(xantphos)(4,4'-$(CF_3)_2$bpy)][PF_6], [Cu(xantphos)(5,5'-$(CF_3)_2$bpy)][PF_6] and [Cu(xantphos)(6,6'-Me_2-4,4'-$(CF_3)_2$bpy][PF_6].

The highest powder PLQY was measured for [Cu(xantphos)(6,6'-Me_2-4,4'-$(CF_3)_2$bpy)][PF_6] (PLQY = 50.3%). Due to this high quantum yield, the emission in the photograph in Figure 6 appears to be almost white, whereas according to the CIE coordinates (0.449, 0.532, see also Figure S12), the colour of the emitted light is between the green and the yellow region. For all the complexes, the emission maxima are blueshifted on going from solution to solid state, which has been observed in earlier studies of similar compounds.[16] In general, the emissive properties of the complexes are enhanced in solid state compared to solution. The only complex with a noteworthy quantum yield in solution is [Cu(xantphos)(6,6'-Me_2bpy)][PF_6] with 1.6 versus 10.0% for non-deaerated and deaerated solutions. The higher solution quantum yield is usually attributed to the steric protection of the copper(I) centre by the methyl groups attached to the bpy, which also help to avoid tetrahedron flattening. It is therefore surprising that the PLQY of [Cu(xantphos)(6,6'-Me_2-4,4'-$(CF_3)_2$bpy)][PF_6] in solution (0.5%, Table 3) is two orders of magnitude lower than in powder (50.3%) and also significantly lower than the PLQY of [Cu(xantphos)(6,6'-Me_2bpy)][PF_6]. It appears that although the methyl groups should retain a beneficial effect, this is cancelled out in solution by the CF_3 groups in 4,4'-positions, which seem to offer additional non-radiative pathways in solution and thus quench the excited state. The effect on the photophysical properties of substitution with CF_3 groups in the 4,4'-positions of the bpy is therefore rather ambiguous. Whereas in solution the CF_3 groups lead to a weakening and redshift of the emission, in solid state the emission is only redshifted and less intense for [Cu(POP)(4,4'-$(CF_3)_2$bpy)][PF_6] and [Cu(xantphos)(4,4'-$(CF_3)_2$bpy)][PF_6], but for [Cu(xantphos)(6,6'-Me_2-4,4'-$(CF_3)_2$bpy)][PF_6] it is blueshifted and increased even in comparison to [Cu(xantphos)(6,6'-Me_2bpy)][PF_6].

In order to probe the emission processes further, low temperature lifetime and emission spectra of the complexes were recorded. Solutions of the compounds in Me-THF form a glass at 77 K and this approximates to the situation in the solid state. The emission spectra of the complexes with xantphos (with the exception of [Cu(xantphos)(5,5'-$(CF_3)_2$bpy)][PF_6], see above) are illustrated in Figure 7 and the maxima and lifetime values are summarized in Table 3 and compared to the room temperature values of the powder (Table S4).

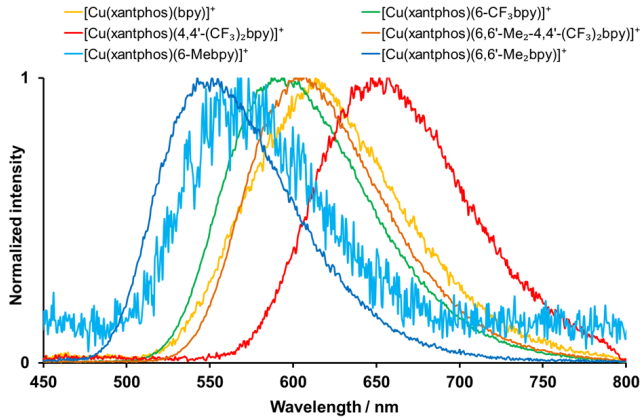

Figure 7. Normalized emission spectra of [Cu(P^P)(N^N)][PF_6] complexes in Me-THF at 77 K, λ_{exc} = 410 nm.

The excited state lifetimes are found to be lengthened for all the complexes, which indicates that they are, as confirmed for similar compounds, TADF emitters.[11, 32, 33] TADF describes the emission from the singlet excited state S_1 which has been (re)populated from the long-lived triplet excited state T_1 by making use of the available thermal energy k_BT. This process is favourable for the application of a molecule as an emitter for two reasons. First, the repopulation of the singlet excited state allows the harvesting of, in theory, 100% of all photons, which equals a PLQY of 100%, respectively all excitons when the situation in the electroluminescent device is considered. Second, TADF processes lead to a shortening of the excited state lifetime. Phosphorescence from T_1 can be a very slow process in comparison to fluorescence from S_1 and is therefore not ideal when it comes to the application of the molecule in light-emitting devices.

At 77 K, TADF is reduced or even completely impeded, depending on the energy gap between T_1 and S_1. As a consequence, the contribution of the slower phosphorescence to the emission is increased, which can be directly evidenced by the significant elogation of the lifetime. This is up to 88 µs for [Cu(xantphos)(6,6'-Me_2bpy)][PF_6], which is an almost eight-fold increase with respect to powder at room temperature (11.4 µs). For [Cu(xantphos)(6,6'-Me_2-4,4'-$(CF_3)_2$bpy)][PF_6], which has a powder lifetime (12.0 µs) similar to [Cu(xantphos)(6,6'-Me_2bpy)][PF_6], the lifetime at 77 K is only less than four-fold increased to 42 µs (Table S4). This could be either due to a shorter phosphorescence lifetime or a smaller energy gap between the triplet and singlet excited states. This energy gap can also be inferred by comparing the powder emission maxima at room temperature and the emission in the frozen Me-THF glass at 77 K. As with lower temperature the proportion of triplet emission increases, the emission maxima should normally be moved to longer wavelengths. This is the case for all the complexes reported here, except for [Cu(xantphos)(5,5'-$(CF_3)_2$bpy)][PF_6], where the emission maximum is basically unchanged, and [Cu(POP)(4,4'-$(CF_3)_2$bpy)][PF_6], with a blueshift of 14 nm (40 meV). The redshift for the other complexes indicates that at room temperature, the majority of the emission stems from the singlet state. The largest redshift is observed for [Cu(xantphos)(6,6'-Me_2-4,4'-$(CF_3)_2$bpy)][PF_6] (345 meV, 87 nm).

To understand the emission processes more thoroughly, the effects of geometry relaxation on the lowest-energy S_1 and T_1 states were investigated theoretically. The geometries of the T_1 states were first optimized at the spin-unrestricted UB3LYP level and they feature relevant differences with respect to those calculated for the ground state S_0. As explained above, T_1 originates in the HOMO→LUMO excitation and implies a charge transfer from a *d* orbital of the Cu atom to a molecular orbital centred on the bpy moiety of the complexes. The metal centre is hence partially oxidized and tends to adopt a squared-planar coordination sphere, typical of four-fold coordinated d^9 copper complexes, instead of the tetrahedral coordination preferred by d^{10} copper complexes. This tendency is clearly illustrated by the angle formed by the N–Cu–N and P–Cu–P planes that changes from values close to 90° in S_0, typical of a tetrahedral coordination in which both ligands are orthogonal, to values as low as 58° in T_1 (Table S1). The presence of substituents in 6,6'-positions hinders the bending of the bpy moiety and limits the flattening distortion of the tetrahedron in T_1. Thus, complexes with one of those positions substituted by a Me or a CF_3 present an angle between the planes through N–Cu–N and P–Cu–P between 70.3 and 71.4°, which is significantly larger than for complexes with no substituent in the 6,6'-positions (~50°). The complexes [Cu(xantphos)(6,6'-Me_2bpy)]$^+$ and [Cu(xantphos)(6,6'-Me_2-4,4'-$(CF_3)_2$bpy]$^+$ with both positions substituted by Me groups present even less flattened structures with angles of 74.3 and 74.4°, respectively (Table S1).

The flattening of the complex structure is accompanied by a large stabilization of the T_1 state that, for complexes with no substituent in 6,6'-positions of the bpy, amounts to 0.8–0.9 eV with respect to the energies at the equilibrium geometry of S_0. This relaxation energy decreases to ~0.6 eV for [Cu(xantphos)(6,6'-Me_2bpy)]$^+$ and [Cu(xantphos)(6,6'-Me_2-4,4'-$(CF_3)_2$bpy)]$^+$ due to the hindering effect of the Me groups that limits the geometrical relaxation. Therefore, the energy position of the T_1 state relative to S_0 not only depends on the electron-donating or electron-withdrawing character of the substituent groups but also on the positions on the ligands where they are introduced due to the purely structural effects they induce. This justifies the fact that the emission maxima recorded for the family of complexes studied does not follow the trends observed for absorption (see above), and also explains that the TD-DFT energies computed for T_1 (Table 4) do not

reproduce the experimental trends observed in the emission spectra because they are based only on electronic considerations (they are calculated at the geometry of S_0) with no geometry relaxation. When the emission energies from T_1 are determined as the vertical energy difference between the T_1 and S_0 states at the T_1 relaxed geometry, they fully support the experimental trends observed at 77 K where TADF is suppressed and emission mainly results from phosphorescence from T_1. $[Cu(POP)(bpy)]^+$, $[Cu(xantphos)(bpy)]^+$ and $[Cu(POP)(6\text{-}CF_3bpy)]^+$ are calculated to emit at very similar wavelengths (730, 737 and 735 nm, respectively) whereas the emission of $[Cu(xantphos)(6\text{-}CF_3bpy)]^+$ is blueshifted (691 nm) and that of complexes with 4,4'- and 5,5'-$(CF_3)_2$bpy is redshifted (1.34–1.41 eV, 920–875 nm). Complex $[Cu(xantphos)(6,6'\text{-}Me_2\text{4,4'-}(CF_3)_2bpy)]^+$, whose absorption wavelength and S_1 energy were shifted to the red with respect to $[Cu(xantphos)(bpy)]^+$, features a T_1 energy (1.80 eV, 688 nm) and a emission maximum at 77 K (2.05 eV, 604 nm) bluer than the reference complex (1.68 and 2.01 eV, respectively). The theoretical values underestimate the experimental emission energies (Table 3) because they are calculated at the fully relaxed geometry of T_1 whereas this relaxation is expected to be severely restricted in the glass at 77 K. As a conclusion, the emission energies of $[Cu(P\text{^}P)(bpy)]^+$ complexes with substituents at 6,6'-positions of the bpy do not correspond to those expected from electronic considerations (MO analysis or electrochemical and optical absorption gaps) because 6,6'-substitution hinders the tetrahedron flattening associated to T_1 relaxation and limits its stabilization. The T_1 state therefore stays at higher energies than in complexes with no substituent at 6,6'-positions, thus leading to a bluer emission than expected.

Finally, the S_1 and T_1 states were fully optimized using the TD-DFT approach to evaluate the adiabatic energy difference ($\Delta E(S_1 - T_1)$) between these states at their respective minimum-energy geometries. It should be mentioned that the complexes in the S_1 state undergo flattening distortions of the tetrahedral structure similar to those discussed above for T_1 because both states originate in the HOMO→LUMO excitation. The values of $\Delta E(S_1 - T_1)$ were computed for a set of representative complexe cations ($[Cu(POP)(bpy)]^+$, $[Cu(xantphos)(bpy)]^+$, $[Cu(POP)(4,4'\text{-}(CF_3)_2bpy)]^+$, $[Cu(xantphos)(4,4'\text{-}(CF_3)_2bpy)]^+$ and $[Cu(xantphos)(6,6'\text{-}Me_2\text{-}4,4'\text{-}(CF_3)_2bpy)]^+$) and in all cases are found in the 0.12–0.20 eV range. These values are significantly lower than the 0.37 eV (3000 cm^{-1}) proposed by Yersin and coworkers.[12,34] to allow the population of S_1 from T_1 at room temperature and, therefore, contribution from S_1 to the emission by TADF should be expected at room temperature. The ΔE values calculated for the reference complexes $[Cu(POP)(bpy)]^+$ and $[Cu(xantphos)(bpy)]^+$ are 0.177 and 0.185 eV, respectively, slightly above the ideal value of 0.12 eV for TADF being exploited in electroluminescent devices, but still in the range of other Cu complexes for which TADF has been reported previously. The inclusion of CF_3 groups in the 4,4'-positions has little effect on ΔE that slightly increases for $[Cu(POP)(4,4'\text{-}(CF_3)_2bpy)]^+$ (0.189 eV) and $[Cu(xantphos)(4,4'\text{-}(CF_3)_2bpy)]^+$ (0.197 eV). However, the addition of Me groups in 6,6'-positions favours a decrease in ΔE, and the value of 0.110 eV computed for $[Cu(xantphos)(6,6'\text{-}Me_2\text{-}4,4'\text{-}(CF_3)_2bpy)]^+$ points to this complex as the one expected to feature TADF at lower temperatures.

Electroluminescent devices

Light-emitting electrochemical cells (LECs) were fabricated with complexes $[Cu(POP)(6\text{-}CF_3bpy)][PF_6]$, $[Cu(xantphos)(6\text{-}CF_3bpy)][PF_6]$ and $[Cu(xantphos)(6,6'\text{-}Me_2\text{-}4,4'\text{-}(CF_3)_2bpy)][PF_6]$ because only these CF_3-substituted complexes show significant PLQY values in powder (6.2, 11.1 and 50.3%, respectively, Table 3). The LECs were fabricated in a double layer architecture, by depositing a poly(3,4-ethylenedioxythiophene):poly(styrenesulfonate) (PEDOT:PSS) layer and the emissive layer sandwiched between indium tin oxide (ITO) and aluminium electrodes. The active layer contained the copper(I) complex mixed with the ionic liquid (IL) 1-ethyl-3-methylimidazolium hexafluoridophosphate $[Emim][PF_6]$ at a 4:1 (Cu complex:IL) molar ratio. The IL was added to shorten the turn-on time of the LEC by increasing the

Table 5. Performance of ITO/PEDOT:PSS/$[Cu(P\text{^}P)\text{^}N\text{^}N)][PF_6]$:$[Emim][PF_6]$ 4:1 molar ratio/Al LECs measured using a pulsed current driving (average current density 100 A m^{-2}, 1 kHz, 50% duty cycle, block wave).

Complex	t_{on} [a] / min	Lum_0 [b] /cd m^{-2}	Lum_{max} [c] /cd m^{-2}	$t_{1/2}$ [d] / h	EQE_{max} [e] / %	PCE_{max} [f] /lm W^{-1}	$Efficacy_{max}$ / cd A^{-1}	λ_{EL}^{max} / nm
$[Cu(POP)(6\text{-}CF_3bpy)][PF_6]$	22	39	65	8.5	0.4	0.2	0.7	595
$[Cu(xantphos)(6\text{-}CF_3bpy)][PF_6]$	137	5	109	31.0	0.5	0.4	1.1	589
$[Cu(xantphos)(6,6'\text{-}Me_2\text{-}4,4'\text{-}(CF_3)_2bpy)][PF_6]$	8	59	131	2.0	0.6	0.4	1.3	593

[a] Time to reach the maximum luminance. [b] Initial luminance. [c] Maximum luminance reached. [d] Time to reach one-half of the maximum luminance. [e] Maximum external quantum efficiency reached. [f] Maximum power conversion efficiency reached.

concentration of ionic species and thereby the ionic mobility in the light-emitting layer.[35,36] To enhance the device response and lifetime, LECs were operated using a block-wave pulsed current of 100 A m^{-2} (1 kHz and 50% duty). The LEC characteristics are summarized in Table 5 and the luminance and average voltage versus time plots are depicted in Figure 8 and S13, respectively.

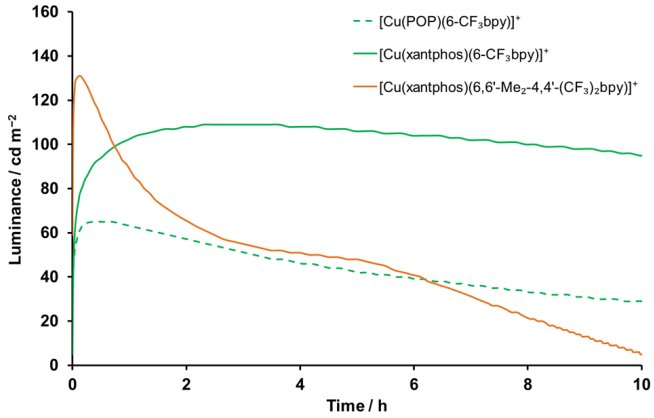

Figure 8. Luminance versus time characteristics for ITO/PEDOT:PSS/[Cu(P^P)^N^N)][PF_6]:[Emim][PF_6] 4:1/Al LECs operated at pulsed current (average current density 100 A m^{-2}, 1 kHz, 50% duty cycle, block wave).

All three LECs have orange electroluminescence (Figure S14) with maximum emission in the 589–595 nm range and a shoulder around 650 nm similar to that observed for the spectra in solution (Figure 4). The emission maxima are slightly blue-shifted with respect to the photoluminescence spectra recorded for the active thin film (Cu complex:IL at a 4:1 molar ratio) with maxima in the 596–606 nm range (Figure S15). It should be noted that the PLQY significantly decreases in passing from powder to the active thin film composition for both [Cu(POP)(6-CF_3bpy)][PF_6] (PLQY = 4%), [Cu(xantphos)(6-CF_3bpy)][PF_6] (5%) and especially for [Cu(xantphos)(6,6'-Me_2-4,4'-$(CF_3)_2$bpy)][PF_6] (16%). This decrease in PLQY has been observed for Cu-based emitters and is related to the different environment surrounding the complex.[16,18] In thin amorphous films, the structural rearrangement of the complex upon excitation is less hindered than in powder which leads to poorer emissive properties. The presence of the CF_3 group results in a slight red-shift of the electroluminescence when comparing to the analogous complexes substituted with methyl groups [Cu(POP)(6-Mebpy)][PF_6] (λ_{EL}^{max} = 574 nm)[15] and [Cu(xantphos)(6-Mebpy)][PF_6] (λ_{EL}^{max} = 583 nm).[16]

Once biased, the electrical resistance of the device is reduced due to the presence of ions in agreement with the operational mechanism established for LECs.[37] Hence, the luminance is initially low and rises up gradually (Figure 8). The time needed to achieve the maximum luminance (t_{on}) is an indicator of the device response, and the operational lifetime ($t_{1/2}$) is usually defined as the time to reach one-half of the maximum luminance. The LEC containing [Cu(xantphos)(6,6'-Me_2-4,4'-$(CF_3)_2$bpy)][PF_6] has the shortest t_{on} (8 min) and $t_{1/2}$ (2h). When the active material is [Cu(POP)(6-CF_3bpy)][PF_6] or [Cu(xantphos)(6-CF_3bpy)][PF_6], the device response is slower with t_{on} values of 22 and 137 min, respectively. Following this trend, the respective LEC lifetimes are 8.5 and 31 hours when using these two complexes (Table 5). These values indicate a clear link between the t_{on} and $t_{1/2}$; the faster the t_{on} the shorter is $t_{1/2}$. On the one hand, the LEC with [Cu(xantphos)(6-CF_3bpy)][PF_6] (with shorter t_{on} and $t_{1/2}$) rapidly reaches its minimum voltage (~4.8 V) which then increases over time (see Figure S13). This voltage profile is indicative of a fast ionic mobility at the beginning of operation. However, over time, charge transport is hindered as evidenced by an increasing resistance during operation. On the other hand, the LEC with [Cu(xantphos)(6-CF_3bpy)][PF_6] shows a voltage profile which decreases over time during device operation.The luminance as well as the efficacy of the LECs are in agreement with the trend obtained for the PLQY in thin film. [Cu(xantphos)(6,6'-Me_2-4,4'-$(CF_3)_2$bpy)][PF_6] with a PLQY of 16% achieves a maximum luminance of 131 cd m^{-2} and a maximum efficacy of 1.3 cd A^{-1}). [Cu(POP)(6-CF_3bpy)][PF_6] with a PLQY of 4% achieves 65 cd m^{-2} and 0.7 cd A^{-1} in the LEC. However, the LEC using [Cu(xantphos)(6-CF_3bpy)][PF_6], with a PLQY of 5% in thin film similar to [Cu(POP)(6-CF_3bpy)][PF_6], exhibits a higher performance with a luminance (109 cd m^{-2}) and a efficacy (1.1 cd A^{-1}) similar to [Cu(xantphos)(6,6'-Me_2-4,4'-$(CF_3)_2$bpy)][PF_6]. Considering the PLQY values in thin film and a typical outcoupling of 20%, the theoretical maximum external quantum efficiency (EQE_{max}) predicted for LECs with [Cu(xantphos)(6-CF_3bpy)][PF_6] and [Cu(xantphos)(6,6'-Me_2-4,4'-$(CF_3)_2$bpy)][PF6] when all injected electrons and holes combine is 1 and 3.2%, respectively, whereas the experimental values are 0.5 and 0.6% (Table 5). The smaller difference found between the theoretical and the experimental value for the LEC with [Cu(xantphos)(6-CF_3bpy)][PF_6] indicates a lower exciton-quenching, which is probably related with a better balance between electrons and holes in the device.[38] With this in mind, together, the time-dependence characteristics and the voltage profile indicate that the characteristics of the LEC with [Cu(xantphos)(6-CF_3bpy)][PF_6] are limited by permanent degradation while with [Cu(xantphos)(6-CF_3bpy)][PF_6] the doping-induced quenching is the main decay factor.

Similar complexes with xanthphos, [Cu(xantphos)(6-Mebpy)][PF_6] and [Cu(xantphos)(6,6'-Me_2bpy)][PF_6], have been previously characterized with the same composition and architecture in LECs but operated with a lower pulsed current (50 A m^{-2}).[16] Compared with [Cu(xantphos)(6-CF_3bpy)][PF_6], substitution of the CF_3 group by a Me group leads to a LEC device with a slightly shorter t_{on} (102 min) but also a reduced $t_{1/2}$

(15 h). The attachment of the second methyl group (6,6'-Me_2bpy) reduces the response time (10 min) but also the lifetime $t_{1/2}$ (0.8 h) of the LEC. Further substitution with CF_3 groups in the 4,4'-positions (6,6'-Me_2-4,4'-$(CF_3)_2$bpy) has benefits on the time-dependence characteristics of the LEC because both the t_{on} (8 min) and $t_{1/2}$ (2 h) are improved with respect to [Cu(xantphos)(6,6'-Me_2bpy)][PF_6], even if the device is operated at higher current densities (100 A m^{-2} vs. 50 A m^{-2}). However, the presence of CF_3 groups is detrimental for both the luminance and the efficiency of the device, which are less for the LEC with [Cu(xantphos)(6,6'-Me_2bpy-4,4'-$(CF_3)_2$)][PF_6] (131 cd m^{-2} and 1.3 cd A^{-1}, respectively) than with [Cu(xantphos)(6,6'-Me_2bpy)][PF_6] (145 cd m^{-2} and 3.0 cd A^{-1}).[16] This negative effect is due to the lower PLQY of the CF_3-substituted emitters in the active films.

Conclusions

We have investigated a series of heteroleptic [Cu(POP)(N^N)][PF_6] and [Cu(xantphos)(N^N)][PF_6] complexes in which the N^N ligand is a bpy substituted with CF_3 groups in either the 6-, 5- or 4-positions. The effects of incorporating both methyl and trifluoromethyl into the bpy domain on the structural, electrochemical and photophysical properties of the complexes have been studied. The single crystal structures of [Cu(xantphos)(bpy)][PF_6], [Cu(xantphos)(4,4'-$(CF_3)_2$bpy)][PF_6] [Cu(POP)(6-CF_3bpy)][PF_6]·1.3Et_2O·0.35H_2O, [Cu(xantphos)(6-CF_3bpy)][PF_6]·2Et_2O·1.5CH_2Cl_2, [Cu(POP)(4,4'-$(CF_3)_2$bpy)][PF_6]·0.5CH_2Cl_2 and [Cu(POP)(5,5'-$(CF_3)_2$bpy)][PF_6]·0.5Et_2O have been determined; each copper(I) centre is in a distorted tetrahedral environment.

Introducing the CF_3 groups pushes the value of $E_{1/2}^{ox}$ for the Cu^+/Cu^{2+} process to higher potentials (+0.85 to +0.96 V) with respect to [Cu(POP)(bpy)]$^+$ and [Cu(xantphos)(bpy)]$^+$, and the observed trends in $E_{1/2}^{ox}$ are consistent with results of DFT calculations. The HOMO–LUMO separation is significantly altered by the nature of the N^N ligand, with the largest redshift in the MLCT band being for [Cu(P^P)(5,5'-$(CF_3)_2$bpy)]$^+$; this observation is corroborated by DFT calculations. In solution, the compounds are weak yellow to red emitters, but the emission is enhanced on going to the solid state. Powdered [Cu(xantphos)(4,4'-$(CF_3)_2$bpy)][PF_6] (λ_{em}^{max} = 517 nm) exhibits the highest PLQY (50.3%). The emission properties strongly depend on the substitution pattern and cannot be explained by simple electronic considerations due to the flattening of the tetrahedral structure experienced by the complex upon excitation. Compared to solution behaviour at 298 K, excited state lifetimes lengthen for all complexes in frozen Me-THF (77 K), which is indicative of TADF. TD-DFT calculations reveal that $\Delta E(S_1 - T_1)$ lies in the range 0.12–0.20 eV, which is a small enough energy to allow TADF.

LECs were fabricated with [Cu(POP)(6-CF_3bpy)][PF_6], [Cu(xantphos)(6-CF_3bpy)][PF_6] or [Cu(xantphos)(6,6'-Me_2-4,4'-$(CF_3)_2$bpy)][PF_6] in the emissive layer. All showed yellow electroluminescence (λ_{em}^{max} = 589–595 nm). The LEC with [Cu(xantphos)(6,6'-Me_2-4,4'-$(CF_3)_2$bpy)][PF_6] had the fastest turn-on time (8 min), whereas the longest lived LEC ($t_{1/2}$ = 31 h) contained [Cu(xantphos)(6-CF_3bpy)][PF_6]; these LECs reached maximum luminances of 131 and 109 cd m^{-2} respectively. Although the device with [Cu(xantphos)(6-CF_3bpy)][PF_6] was operated at higher current density (100 A m^{-2} vs. 50 A m^{-2}), its lifetime $t_{1/2}$ is more than twice as long as for the device with the respective [Cu(xantphos)(6-Mebpy)][PF_6] complex (31 vs. 15 h). However, compared to LECs with CF_3-free bpy-based [Cu(POP)(N^N)]$^+$ or [Cu(xantphos)(N^N)]$^+$ complexes, those incorporating CF_3 groups performed less well; CF_3 substituents are detrimental to both the luminance and the efficiency of the LEC.

Acknowledgements

Financial support from the Swiss National Science Foundation (Grant number 162631), the University of Basel, the MINECO of Spain (CTQ2015-71154-P and Unidad de Excelencia María de Maeztu MDM-2015-0538), the Generalitat Valenciana (PROMETEO/2016/ 135) and European FEDER funds (CTQ2015-71154-P) is acknowledged. Prof. Dr. Oliver S. Wenger and Dr. Christopher Bryan Larsen are thanked for use of their LP920-KS instrument from Edinburgh Instruments, including Quantel Brilliant b Nd:YAG laser and iCCD camera from Andor, for low-temperature emission and lifetime measurements.

Keywords: copper • 2,2'-bipyridine • chelating bis(phosphane) • trifluoromethyl • light-emitting electrochemical cell

1 N. T. Kalyani, H. Swart, S. J. Dhoble, *Principles and Applications of Organic Light Emitting Diodes (OLEDs)*, Woodhead Publishing, Duxford, United Kingdom, **2017**.

2 Yi-Lu Chang, *Efficient Organic Light Emitting-Diodes (OLEDs)*, CRC Press Taylor&Francis group, Boca Raton, Florida, **2016**.

3 H. Yersin, *Highly Efficient OLEDs with Phosphorescent Materials*, Wiley-VCH Verlag GmbH & Co. KGaA, Weinheim, Germany, **2008**.

4 H. Rudmann, S. Shimada, M. F. Rubner, *J. Am. Chem. Soc.* **2002**, *124*, 4918-4921.

5 R.D. Costa, E. Ortí, H.J. Bolink, F. Monti, G. Accorsi, N. Armaroli, *Angew. Chem. Int. Ed.* **2012**, *51*, 8178-8211.

6 C. E. Housecroft, E.C. Constable, *Coord. Chem. Rev.* **2017**, *350*, 155-177.

7 H. J. Bolink, E. Coronado, R. D. Costa, N. Lardiés, E. Ortí, *Inorg. Chem.* **2008**, *47*, 9149-9151.

8 R. D. Costa, E. Ortí, H. J. Bolink, S. Graber, C. E. Housecroft, E. C. Constable, *Adv. Funct. Mater.* **2010**, *20*, 1511-1520.

9 K. J. Suhr, L. D. Bastatas, Y. Shen, L. A. Mitchell, B. J. Holliday, J. D. Slinker, *ACS Appl. Mater. Interfaces* **2016**, *8*, 8888-8892.

10 See for example: C. E. Housecroft and E. C. Constable, *Chem. Soc. Rev.* **2015**, *44*, 8386-8398.

11 R. Czerwieniec, H. Yersin, *Inorg. Chem.* **2015**, *54*, 4322-4327.

12 R. Czerwieniec, M. J. Leitl, H. H. H. Homeier, H. Yersin, *Coord. Chem. Rev.* **2016**, *325*, 2-28.

13 L. Bergmann, G. J. Hedley, T. Baumann, S. Bräse, I. D.W. Samuel, *Sci. Adv.* **2016**, *2*, e1500889.

14. M. Osawa, M. Hashimoto, I. Kawata, M. Hoshino, *Dalton Trans.* **2017**, *46*, 12446-12455.

15 S. Keller, E. C. Constable, C. E. Housecroft, M. Neuburger, A. Prescimone, G. Longo, A. Pertegás, M. Sessolo, H. J. Bolink, *Dalton Trans.* **2014**, *43*, 16593-16596.

16 S. Keller, A. Pertegás, G. Longo, L. Martinez, J. Cerdá, J. M. Junquera-Hernández, A. Prescimone, E. C. Constable, C. E. Housecroft, E. Ortí, H. J. Bolink, *J. Mater. Chem. C.* **2016**, *4*, 3857-3871.

17 M. D. Weber, M. Viciano-Chumillas, D. Armentano, J. Cano, R. D. Costa, *Dalton Trans.* **2017**, *46*, 6312-6323.

18 F. Brunner, L. Martínez-Sarti, S. Keller, A. Pertegás, A. Prescimone, E. C. Constable, H. J. Bolink, C. E. Housecroft, *Dalton Trans.* **2016**, *45*, 15180-15192.

19 Y. Chi, B. Tong, P.-T. Chou, *Coord. Chem. Rev.* **2014**, *281*, 1-25.

20 F. Brunner, Y. M. Klein, S. Keller, C. D. Morris, A. Prescimone, E. C. Constable, C. E. Housecroft, *RSC Adv.* **2015**, *5*, 58694-58703.

21 D. O'Hagana, H. S. Rzepa, *Chem. Commun.* **1997**, 645-652 and references therein.

22 I. Andrés-Tomé, J. Fyson, F.B. Dias, A.P. Monkman, G. Iacobellis, P. Coppo, *Dalton Trans.* **2012**, *41*, 8669-8674.

23 J. Yuasa, M. Dan, T. Kawai, *Dalton Trans.* **2013**, *42*, 16096-16101.

24 M. W. Mara, K. A. Fransted, L. X. Chen, *Coord. Chem. Rev.* **2015**, *282-283*, 2-18.

25 M. Tromp, A. J. Dent, J. Headspith, T. L. Easun, X.-Z. Sun, M. W. George, O. Mathon, G. Smolentsev, M. L. Hamilton, J. Evans, *J. Phys. Chem. B* **2013**, *117*, 7381-7387.

26 T. J. Penfold, S. Karlsson, G. Capano, F. A. Lima, J. Rittmann, M. Reinhard, M. H. Rittmann-Frank, O. Braem, E. Baranoff, R. Abela, I. Tavernelli, U. Rothlisberger, C. J. Milne, M. Chergui, J. *Phys. Chem. A* **2013**, *117*, 4591-4601.

27 A. Kaeser, M. Mohankumar, J. Mohanraj, F. Monti, M.Holler, J.-J.Cid, O. Moudam, I.Nierengarten, L. Karmazin-Brelot, C. Duhayon, B. Delavaux-Nicot, N. Armaroli, J.-F. Nierengarten, *Inorg. Chem.* **2013**, *52*, 12140-12151.

28 F. Brunner, Y. M. Klein, S. Keller, C. D. Morris, A. Prescimone, E. C. Constable, C. E. Housecroft, *RSC Adv.* **2015**, *5*, 58694-58703.

29 S. Keller, F. Brunner, A. Prescimone, E. C. Constable, C. E. Housecroft, *Inorg. Chem. Comm.* **2015**, *58*, 64-66.

30 M. Charton, *J. Am. Chem. Soc.* **1969**, *91*, 615-618.

31 K. Uneyama, *Organofluorine Chemistry*, Blackwell Publishing, Oxford, UK, **2006**.

32 M. Y. Wong, E. Zysman-Colman in *Light-Emitting Electrochemical Cells*, ed. R. D. Costa, Springer International Publishing AG, Cham, Switzerland, **2017**, pp. 237-266.

33 M. Elie, S. Gaillard, J.-L. Renaud, in *Light-Emitting Electrochemical Cells*, ed. R. D. Costa, Springer International Publishing AG, Cham, Switzerland, **2017**, pp. 287-327.

34 M. J. Leitl, V. A. Krylova, P. I. Djurovich, M. E. Thompson, H. Yersin, *J. Am. Chem. Soc.* **2014**, *136*, 16032-16038.

35 S. T. Parker, J. D. Slinker, M. S. Lowry, M. P. Cox, S. Bernhard, G. G. Malliaras, *Chem. Mater.* **2005,** *17,* 3187-3190.

36 R. D. Costa, A. Pertegás, E. Ortí, H. J. Bolink, *Chem. Mater.* **2010**, *22*, 1288-1290.

37 S. van Reenen, P. Matyba, A. Dzwilewski, R. A. J. Janssen, L. Edman, M. Kemerink, *J. Am. Chem. Soc.*, **2010**, *132*, 13776-13781.

38 H.-C. Su, J.-H. Hsu, *Dalton Trans.* **2015**, *44*, 8330-8345.

FULL PAPER

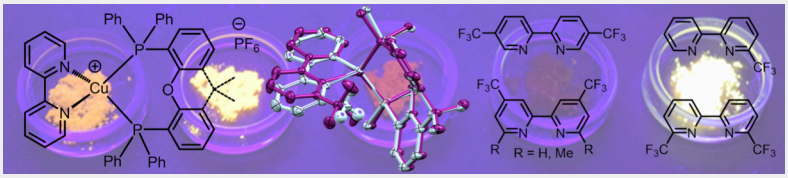

Text for Table of Contents

Sarah Keller, Fabian Brunner, José M. Junquera-Hernández, Antonio Pertegás, Maria-Grazia La-Placa, Alessandro Prescimone, Edwin C. Constable, Henk J. Bolink, Enrique Ortí* and Catherine E. Housecroft*

Page No. – Page No.

CF_3 Substitution of [Cu(P^P)(bpy)][PF_6] Complexes: Effects on Photophysical Properties and Light-emitting Electrochemical Cell Performance

[a] S. Keller, F. Brunner, Dr. A. Prescimone, Pr
Prof. Dr. C.E. Housecroft
Department of Chemistry
University of Basel
BPR 1096, Mattenstrasse 24a, Basel 4058,
E-mail: catherine.housecroft@unibas.ch
[b] Dr. J.M. Junquera-Hernández, Dr. A. Perteg
H.J. Bolink, Prof. Dr. E. Ortí
Instituto de Ciencia Molecular,
Universidad de Valencia,
ES-45980 Paterna, Valencia, Spain
e-mail: enrique.orti@uv.es

Supporting information for this article is give
the document.((Please delete this text if not